Available online at www.sciencedirect.com

ScienceDirect

IFAC PapersOnLine 58-13 (2024) 266–271

Overcurrent Limitation in Hydrogen Storage Power Plants (HSPP)

Nayeemuddin Ahmed, Harald Weber

Electrical Energy Supply (EEV), University of Rostock,
Rostock 18059, Germany
E-mail: (nayeemuddin.ahmed, harald.weber)@uni-rostock.de

Abstract: The importance of electrical energy storage (EES) systems has been increasingly recognized for enabling the large-scale integration of intermittent renewable energy sources (RES) into the power grid. Among these systems, the Hydrogen Storage Power Plant (HSPP) stands out as a solution capable of independently managing the supply and storage of electrical energy based on network requirements. Previous investigations have shown that the HSPP operating in grid forming mode (GFM) can provide the required ancillary services in the form of instantaneous, primary and secondary control reserves similar to conventional fossil-fired power plants. However, unlike these traditional synchronous generators, the HSPP consists of power semiconductor devices, resulting in much lower overcurrent tolerance. This paper addresses this challenge by proposing a simple yet robust control technique that regulates the maximum current across the HSPP grid interfacing inverter functioning in GFM. The results demonstrate that the controller can maintain the maximum current magnitude below a threshold of 1.2 pu while ensuring the required reactive current contribution during a three-phase fault.

Keywords: Ancillary service, grid forming inverter, hydrogen storage, overcurrent, power semiconductor.

1. INTRODUCTION

The primary challenge with RES, such as solar and wind, is their dependence on fluctuating primary resources, leading to inconsistent power generation. Consequently, RES cannot always meet network power demands or provide reliable balancing energy with 100% reliability (Chuang and Schwaegerl (2009)). Currently, conventional power plants (CPP) bridge the gap between varying RES power generation and load consumption. However, due to diminishing fossil fuels and the need to meet climate action targets, there are plans to phase out most CPPs and replace them with RES (German Institute for Economic Research (2019)). Therefore, finding alternative solutions that can provide the same ancillary services as CPPs is increasingly important.

One promising solution is the HSPP, which integrates a system of converters and storage units. This configuration enables the HSPP to supply electrical energy according to grid requirements and store excess energy generated by RES. The HSPP can operate over extended periods, depending on its storage capacity. There are three primary storages, i.e., supercapacitor, battery and hydrogen storage. These storages are ideally suited for providing instantaneous, primary, and secondary control reserves (IR, PCR, SCR), allowing the HSPP to fulfill necessary ancillary service requirements (Gerdun et al. (2019)).

For the HSPP to perform these ancillary services in future grids dominated by RES, it must operate in GFM. This mode allows the power plant to function as a controlled voltage source, establishing system voltage and frequency references independently, which is crucial for maintaining stability in weak grid conditions (Matevosyan et al. (2019)). These reference values are also essential for grid-following inverters in conventional RES to feed the required active and reactive power into the network (Christensen et al. (2020)).

However, the voltage-source behavior of the HSPP inverter makes its output current highly sensitive to external disturbances. During voltage dips or faults at the point of common coupling, the HSPP inverter can experience significant overcurrent for extended periods. Due to the limited overcurrent tolerance of power electronic semiconductors in inverters (1.2–1.5 pu) compared to traditional synchronous generators (5–7 pu), an effective overcurrent protection scheme is essential for the HSPP inverter to meet the Fault Ride Through (FRT) standard (Hooshyar and Iravani (2017); Fan et al. (2022); Johnson (2021)). Additionally, the HSPP must fulfill the requirements for reactive current injection during faults and ensure sufficiently fast post-fault recovery (Christensen et al. (2020); Kay (2020)).

Various overcurrent protection techniques have been proposed, including virtual impedances, current limiters, and voltage limiters (Paquette and Divan (2014); Fan and Wang (2022); Bloemink and Iravani (2012)). While these methods help regulate overcurrent magnitude, each has drawbacks. Virtual impedance can cause a sluggish post-fault response, and current limiters require the inverter to function as a current source instead of a voltage source. Voltage limiters avoid these disadvantages but need additional information about the magnitude and angle of

10.1016/j.ifacol.2024.07.493

voltage reduction to meet reactive current injection requirements during faults (Fan et al. (2022)).

To address these issues, an alternative overcurrent controller is proposed in this paper that not only limits steady-state fault current but also ensures compliance with all FRT conditions. The next section briefly introduces the HSPP components and is followed by a detailed explanation of the implemented overcurrent limitation technique. Finally, the controller's performance is evaluated in the result section, and the research highlights are presented in the conclusion.

2. INTERNAL HSPP STRUCTURE

The internal structure of the HSPP is presented in Fig. 1. In such power plants, following a sudden change in power generation or demand in the three-phase network, IR, PCR and SCR are provided by the three main storages, i.e., supercapacitor, battery and hydrogen storage, respectively (Gerdun et al. (2019); Ahmed et al. (2020); Töpfer et al. (2020)). These three storages have specific properties, enabling them to fulfill their respective tasks. A supercapacitor provides IR since the component can charge and discharge instantaneously with a high power gradient in response to network disturbances. Its ability to undergo frequent charging and discharging cycles makes it an ideal device for inertia emulation. Contrary to the supercapacitor, the battery is suited for PCR provision since it is a cheaper form of storage with a higher energy density. Rapid charging or discharging of the battery is detrimental to its average lifespan, so the use of battery systems for providing IR still needs to be proven. Hence, the combination of the supercapacitor parallel to the battery satisfies the required IR and PCR requirements.

The battery voltage regulates the SCR response from the hydrogen storage. If there is surplus energy in the network, the battery voltage rises and, upon exceeding an upper threshold, activates the electrolyzer path. This leads to the synthesis of hydrogen from the excess energy. Conversely, during increased demand, if the battery voltage reduces beyond a lower threshold after providing PCR, the fuel cell path is activated. SCR provisions are then met by generating electrical energy from stored hydrogen. The power flow is controlled by the respective DC-DC converter between the hydrogen storage and the battery during each situation.

The ability of the HSPP to store and provide electrical energy enables its active power output to be adjusted in response to both positive and negative disturbances, ensuring grid stability. However, for the efficient provision of necessary ancillary services and adherence to grid code regulations, low voltage FRT must also be ensured by the HSPP. Thus, to meet the associated requirements, an overcurrent controller is designed for the power plant, operating on the principles outlined in the following section.

3. OVERCURRENT LIMITATION PRINCIPLE

The principle of current limitation can be illustrated using the simplified system depicted in Fig. 2. Here, the HSPP is linked to an external network via an impedance. It is assumed that both the HSPP and the network operate at a High Voltage (HV) level. At such voltages, the reactance (x) significantly exceeds the resistance (i.e., x >> r). Thus, the impedance can be expressed as follows, using lower-case letters to denote per unit (pu):

$$\bar{z} = r + jx = jx \tag{1}$$

For this system, the sending end reactive power (q_1) and current (i_1) from node 1 can be formulated as:

$$q_1 = \frac{(v_1)^2}{x} - \frac{v_1 \cdot v_2}{x} cos(\delta_1 - \delta_2) \tag{2}$$

$$\bar{i}_1 = \frac{\bar{v}_1 - \bar{v}_2}{jx} \tag{3}$$

Next, a three-phase fault is introduced at node 2 without any fault impedance ($\bar{z}_f = 0$). This alters the network structure as shown in Fig. 3. For this scenario, with the voltage at node 2 ($\bar{v}_2$) set to 0, the HSPP reactive power output (q_{1F}) and corresponding current (i_{1F})are:

$$q_{1F} = \frac{(v_1)^2}{x} \tag{4}$$

$$\bar{i}_{1F} = \frac{\bar{v}_1}{jx} \tag{5}$$

The four equations (2)-(5) can then be represented on the first quadrant of a characteristic plot as shown in Fig. 4. Here, the magnitude of the voltage at node 1 (v_1) and the

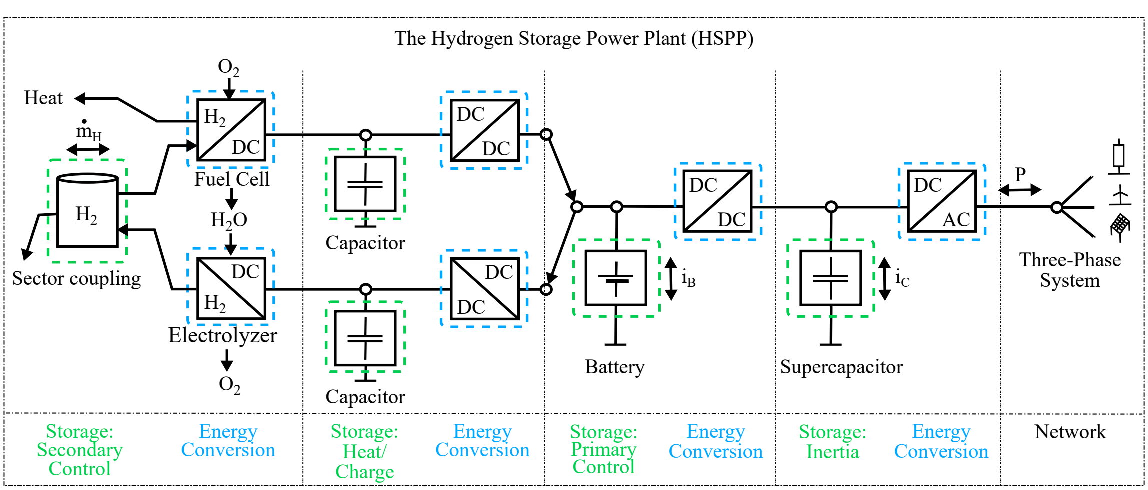

Fig. 1. Working principle of the internal components of a Hydrogen Storage Power Plant (HSPP)

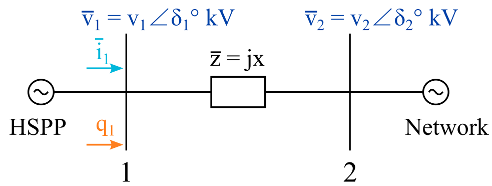

Fig. 2. Simplified pre-fault representation of the HSPP connected to an external network

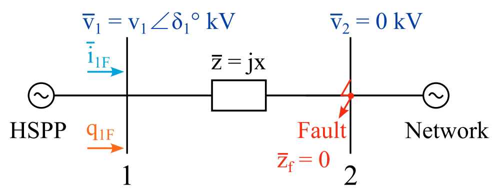

Fig. 3. Representation of the HSPP connected to an external network during fault

real component of the HSPP current (i_r) are represented on the y-axis with different values. Both the sending end reactive power (q) and the imaginary part of the current (i_i) are represented on the x-axis. These two quantities (q & i_i) have opposite polarity since a lagging current (i.e., negative i_i) yields positive reactive power.

As indicated by (4) and (5), q_{1F} and i_{1F} are represented as a horizontal parabola and a linear function, respectively. Similarly, (2) and (3) are incorporated into the plot, assuming that the magnitudes of v_1 and v_2 are approximately equal, and the angle δ_1 is more positive than δ_2, to ensure active and reactive power flow from the HSPP to the network.

The gray lines in Fig. 4 delineate the characteristics of the v-q controller in the HSPP, with the gradient indicating the v-q droop (σ). Functioning as the slack generator, the HSPP supplies the active and reactive power demand of the network. Consequently, its voltage is set to $1.0\underline{/0^\circ}$ in pu. From Fig. 4, the intersection of the v-q characteristic with the q curve at $v_1 = 1$ signifies that the HSPP operates at working point "a" and supplies the corresponding reactive power (q_{10}). Following the same principle, the x-axis value at "a'" yields the pre-fault real and imaginary current components (i_{1r0} & i_{1i0}). Thus, the magnitude of the initial pre-fault (i_{10}) current is:

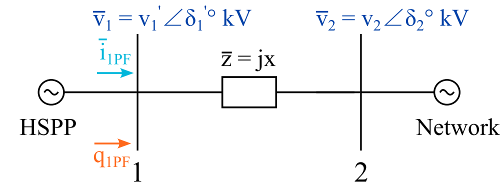

Fig. 5. Post-fault representation of the HSPP connected to an external network

$$i_{10} = \sqrt{(i_{1r0})^2 + (i_{1i0})^2} \tag{6}$$

Fig. 4 can be used further to explain the behavior of the overcurrent controller during the fault. Once the fault occurs, the HSPP behaves as a slack initially and maintains its voltage magnitude (v_1) constant at 1. Consequently, the intersection of this horizontal line with the plots of q_{1F} and i_{1F} leads to the points "b" and "b'", which represent the uncontrolled HSPP reactive power and current output immediately after the fault. It should be noted that in this case, the quantity i_{1F} is scalar and is represented as a function of v_1. It is not plotted as a vector and thus cannot be resolved into its real and imaginary components using the given axes in Fig. 4. The maximum fault current at "b'" consists of only the imaginary part of the current since solely a reactance exists between nodes 1 and 2.

When the system is at point "b", the overcurrent controller significantly reduces the reference reactive power ($q_{ref(min)}$ in Fig. 4). This action decreases the HSPP terminal voltage magnitude from (v_1) to v_1', thereby reducing the fault current. The controller employs a proportional gain to ensure a rapid response, quickly lowering the HSPP reactive power and current magnitude to points "c" and "c'" respectively. Simultaneously, the active power and, consequently, the real current of the HSPP (i_{1rF}) is reduced to 0. Thus, the current magnitude at "c'" consists only of the imaginary current part (i_{1iF}). This configuration maximizes the reactive current support the power plant can provide during the fault.

For the remainder of the fault duration, both the reactive power and current maintain these reduced levels. The current magnitude at "c'" is kept below i_{1max}. This parameter represents the maximum current threshold designed to prevent the violation of the HSPP inverter's thermal limit and can be set to any chosen value (e.g., 1.2 pu). The

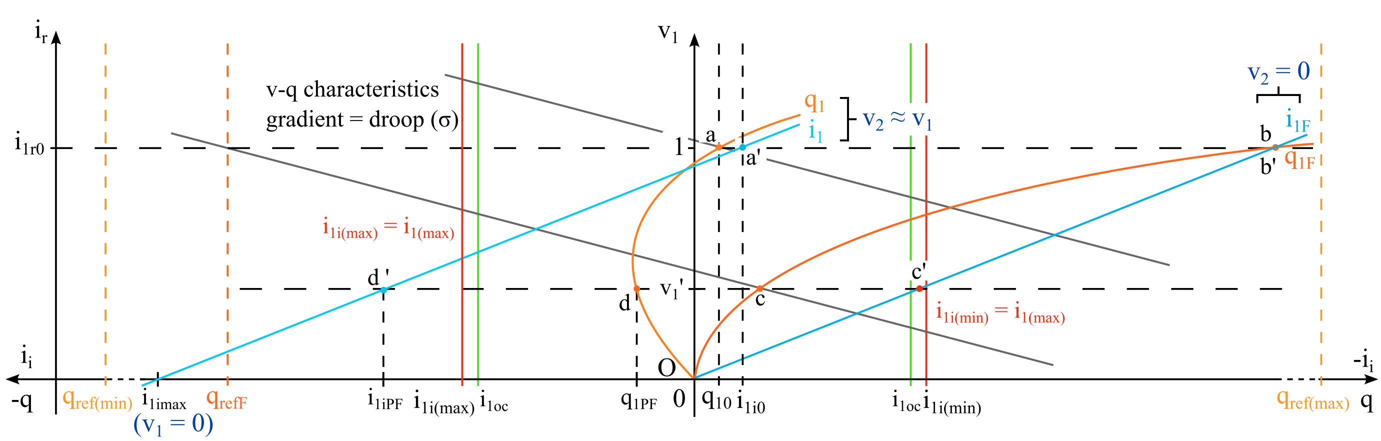

Fig. 4. Overcurrent controller operation (diagram not to scale)

overcurrent regulator employs a current limit i_{1oc}, which is always set lower than i_{1max}. Since a proportional controller is used, the current after the initial step increase settles to a value between i_{1oc} and i_{1max}. This ensures that the output current stays within permissible thresholds.

Once the fault is cleared after a given duration (e.g., 150 ms), the voltage at node 2 is immediately restored to a value close to its nominal magnitude by the strong external network. During this time, the voltage at node 1 remains very low (represented by $v_1{'}\underline{/\delta_1{'}^\circ}$) due to the current-limiting action during the fault. Under these conditions, both the reactive power and current reverse direction and flow from node 2 to node 1. Consequently, the system transitions to points "d" and "d'", as shown in Fig. 4. The corresponding reactive power and current values immediately after the fault clearance are also marked on the axes. Equations 7 and 8 represent the reactive power and current relationships with the nodal voltage magnitudes and angles. The negative values in both cases denote the change in direction, compared to the illustration in Fig. 5.

$$q_{1PF} = \frac{(v_1{'})^2}{x} - \frac{v_1{'} \cdot v_2}{x} cos(\delta_1{'} - \delta_2) \tag{7}$$

$$\bar{i}_{1PF} = \frac{\bar{v}_1 - \bar{v}_2}{jx} \tag{8}$$

The post-fault characteristics are depicted in the second quadrant of Fig. 4. Since point "d'" exceeds the maximum current threshold i_{1max}, a large increase in the reference reactive power (represented as $q_{ref(max)}$ in Fig. 4) is implemented by the overcurrent regulator. This promptly increases the HSPP terminal voltage, thus reducing the current. This rapid change brings the system operating point close to its initial values at "a" and "a'". Once the current is within the tolerance limit of i_{1max}, the overcurrent regulator stops, and the q controller, which employs a slower integral controller, takes over. This latter regulator ensures post-fault recovery by returning the system to its initial working points of "a" and "a'". In summary, the reactive power (q_1) and current (i_1) follow these transitions from the fault inception to the post-fault steady-state-

- q_1: $a \rightarrow b \rightarrow c \rightarrow d \rightarrow a$
- i_1: $a' \rightarrow b' \rightarrow c' \rightarrow d' \rightarrow a'$

This pathway from Fig. 4 can be compared with the simulation results presented in Figs. 12-14 in the next section.

4. RESULT AND OBSERVATION

Initial evaluations of the overcurrent controller were performed using a simple network designed in DIgSILENT PowerFactory, as depicted in Fig. 7. A three-phase short circuit without any fault impedance was implemented at the Point of Common Coupling (PCC) bus at 1 s. The short circuit lasted for 150 ms, after which it was cleared and the transmission line reconnected. The fault could also have been implemented in the HSPP bus. This would require an impedance between the power plant and its connecting bus. For the current investigations, this impedance is not included, i.e., the HSPP is directly connected to its busbar. The network summary and bus results due to the initial power flow are included in Tables 1 and 2. The apparent power base of the system is 250 MVA.

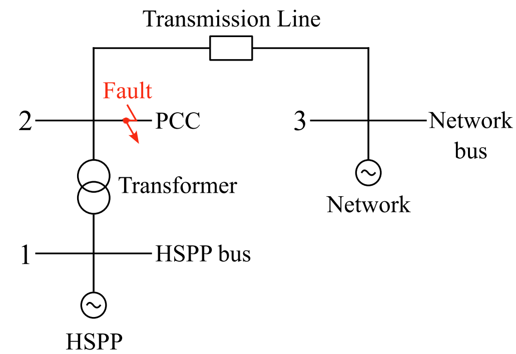

Fig. 7. Investigated network structure

Table 1. Initial power flow summary

Network element or quantity	Active power (pu)	Reactive power (pu)
HSPP	0.80084	0.184
Network	-0.80	-0.080
Active power losses	0.0084	-
Reactive power losses	-	0.104

Table 2. Bus results due to initial power flow

Bus	Nominal voltage (kV)	Voltage (pu)	Current Magnitude (pu)
HSPP	19	$1.0\underline{/0.00^\circ}$	0.822
PCC	380	$0.98\underline{/-7.36^\circ}$	0.822
Network	380	$0.98\underline{/-7.38^\circ}$	0.822

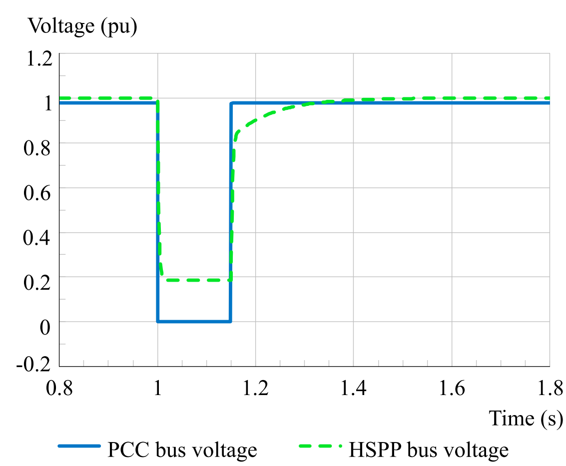

Fig. 8. Terminal voltages of the HSPP and PCC bus

Fig. 8 represents the voltage magnitudes at the PCC and HSPP terminals. Following the fault at 1s, the PCC bus voltage magnitude reduces from 0.98 (as shown in Table 2) to 0 immediately. The HSPP bus voltage remains momentarily at 1 pu. This leads to a high initial flow of short circuit current and reactive power towards the fault location. These increases are shown in Figs. 9 and 10, respectively. The maximum inverter current threshold (i_{max}) is set at 1.2 pu. Since the peak short-circuit significantly surpasses this limit, the proportional overcurrent controller implements a large reduction in the reference

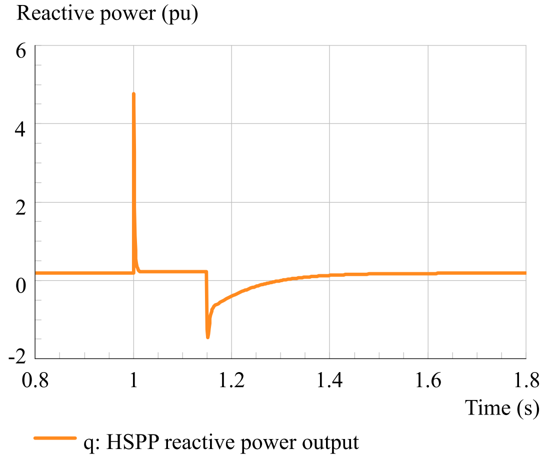

Fig. 9. Reactive power output of the HSPP

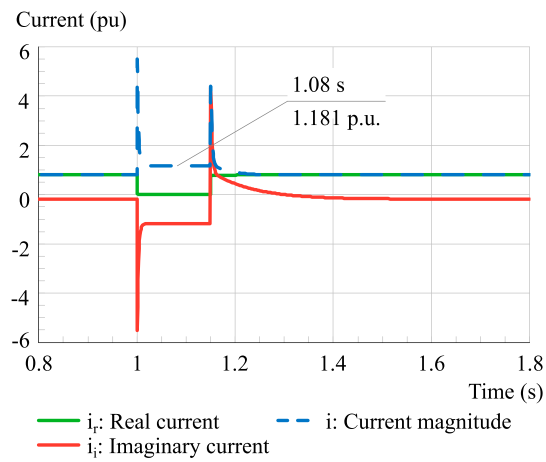

Fig. 10. Real, imaginary and current magnitude outputs from the HSPP

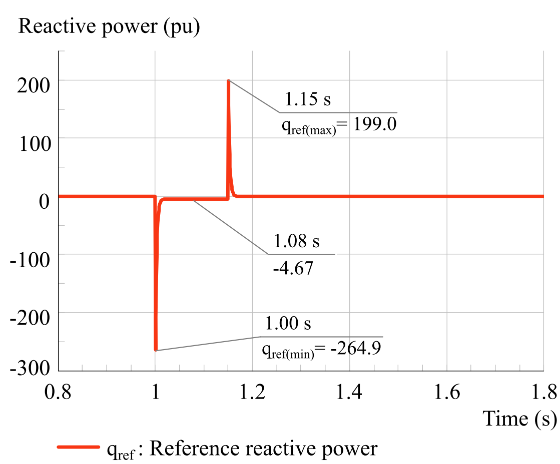

Fig. 11. Reactive power reference of the HSPP

reactive power, labeled as $q_{ref(min)}$ in Fig. 11. This results in a decreased HSPP reactive power output as well as a reduced terminal voltage, as seen in Figs. 8 and 9.

Following the fault clearance, the opposite scenario takes place. The PCC voltage is almost immediately restored to its nominal value by the external grid. Since the PCC voltage is now higher than the terminal voltage of the HSPP, there is a sudden inrush of reactive power and current from the PCC to the HSPP bus. These changes in the reactive power and current can be seen in Figs. 9 and 10 at 1.15s. Once again, the current magnitude limit of 1.2 pu is exceeded. However, due to the post-fault current direction being opposite to the pre-fault current, the overcurrent controller inserts a high increase in the reference reactive power, marked as $q_{ref(max)}$ in Fig. 11. This large positive reference signal reduces the reactive power flow from the PCC to the HSPP bus (negative direction), as shown in Fig. 9. Consequently, the PCC voltage increases sharply, which restores it close to its nominal value, leading to a reduction in the current magnitude. Once the current magnitude is well under the limit of i_{max}, the overcurrent regulator stops functioning. The integral reactive power controller takes over and restores the reactive power, voltage and currents to their prefault values (fault recovery), as shown in Figs. 8-10.

Table 3. Signals and parameters in overcurrent controller

Symbol	Value	Description
q_{ref}	-4.67	Reference reactive power
q_{set}	0.18	Reactive power setpoint (Table 2)
k_{oc}	60	Overcurrent controller gain
i_{oc}	1.1	Overcurrent controller limit
i	-	Current magnitude

Changes in the HSPP current flow are shown in Fig. 10. In accordance with the characteristic diagram in Fig. 4, the pre-fault imaginary current is negative (lagging power factor) while the post-fault imaginary current is positive. However, the current magnitude, being an absolute value, is always shown as positive. During the fault, the real current is reduced to 0, as the controller lowers the active power to 0. This ensures maximum reactive current support during the fault. The current magnitude during the fault is 1.181 per unit. This can be calculated from (9) and the information in Table 3.

$$q_{ref} = q_{set} + k_{oc} \cdot (i_{oc} - i) \tag{9}$$

Fig. 12 displays the HSPP terminal voltage against its reactive output at different time points. The initial reactive power and terminal voltage setpoint are shown at 0 s, followed by the measurements taken after 1 time step (1 ms) of the short circuit. The simulation software requires this time interval after the short circuit takes place at 1 s to perform the necessary calculations. For the same reason, the post-fault measurements are taken at 1.151 s. The diagram shows that it takes the controller only 0.02 s (i.e., 1 s to 1.02 s) to limit the reactive power and the short circuit current. The slower speed of the integral q controller is also apparent between 1.2-1.5 s. This graph can be compared with the pathway of q_1 mentioned at the end of section 3 using Fig. 4).

Fig. 13 summarizes the current results of this investigation, showing the HSPP current magnitude and its terminal voltage at different times. This can be compared with the pathway of i_1 mentioned at the end of section 3. Since the current magnitude is an absolute value, the post-fault current is also shown as a positive value. Reflecting the current path after 1.15 s about the inverter current limit (I_{max}) will yield the same pathway as discussed earlier. An

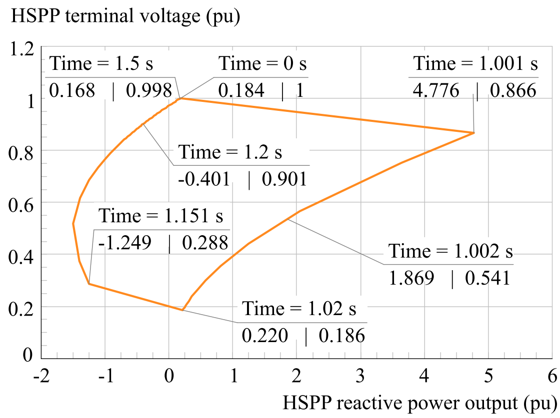

Fig. 12. HSPP voltage against its reactive power output characteristics

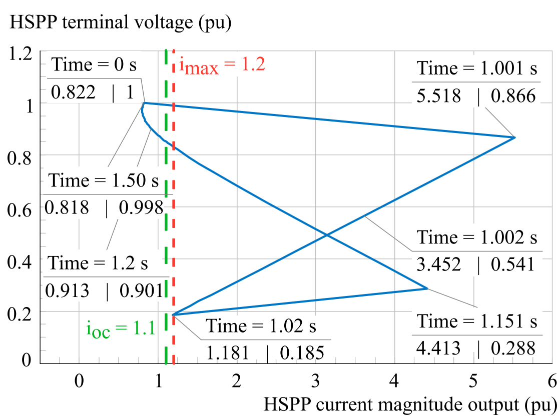

Fig. 13. HSPP voltage against its current magnitude output characteristics

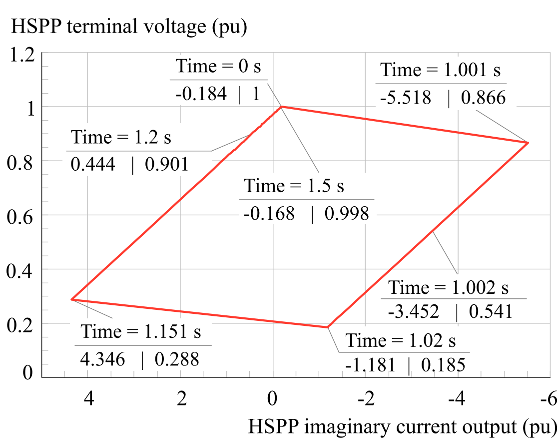

Fig. 14. HSPP voltage against its imaginary current output characteristics

alternative representation involving the imaginary part of the current is presented in Fig. 14 facilitating comparison with the path of i_1 using Fig. 4.

5. CONCLUSION

This paper addresses the critical issue of overcurrent in HSPP inverters operating in GFM. The proposed robust control technique effectively limits the maximum current to below 1.2 pu, ensuring compliance with required FRT standards. The results prove the controller's ability to regulate overcurrent thereby preventing thermal overloads on power semiconductor devices.

Additional investigations are planned to evaluate the controller performance in a larger network involving multiple HSPPs. In addition, the behavior of the internal HSPP components during short circuits also needs to be studied.

REFERENCES

Ahmed, N., Gerdun, P., and Weber, H. (2020). Active power control based on hydrogen availability in a storage power plant. *IFAC-PapersOnLine*, 53(2), 12708–12713.

Bloemink, J.M. and Iravani, M.R. (2012). Control of a multiple source microgrid with built-in islanding detection and current limiting. *IEEE Transactions on Power Delivery*, 27(4), 2122–2132.

Christensen, P., Andersen, G.K., Seidel, M., Bolik, S., Engelken, S., Knueppel, T., Krontiris, A., Wuerflinger, K., Bülo, T., Jahn, J., et al. (2020). High penetration of power electronic interfaced power sources and the potential contribution of grid forming converters.

Chuang, A.S. and Schwaegerl, C. (2009). Ancillary services for renewable integration. In *2009 CIGRE/IEEE PES Joint Symposium Integration of Wide-Scale Renewable Resources Into the Power Delivery System*, 1–1.

Fan, B., Liu, T., Zhao, F., Wu, H., and Wang, X. (2022). A review of current-limiting control of grid-forming inverters under symmetrical disturbances. *IEEE Open Journal of Power Electronics*.

Fan, B. and Wang, X. (2022). Fault recovery analysis of grid-forming inverters with priority-based current limiters. *IEEE Transactions on Power Systems*.

Gerdun, P., Ahmed, N., Vernekar, V., Töpfer, M., and Weber, H. (2019). Dynamic operation of a storage power plant (SPP) with voltage angle control as ancillary service. In *2019 International Conference on Smart Energy Systems and Technologies (SEST)*, 1–6.

German Institute for Economic Research (2019). Phasing out Coal in the German Energy Sector. 45.

Hooshyar, A. and Iravani, R. (2017). Microgrid protection. *Proceedings of the IEEE*, 105(7), 1332–1353.

Johnson, A. (2021). Minimum specification required for provision of gb grid forming (gbgf) capability (formerly virtual synchronous machine/vsm capability). *Nat. Grid ESO, Warwick, UK, Final Modification Rep. GC*, 137.

Kay, M. (2020). Fast fault current injection specification text. *Nat. Grid ESO, Warwick, UK, Final Modification Rep. GC*, 111.

Matevosyan, J., Badrzadeh, B., Prevost, T., Quitmann, E., Ramasubramanian, D., Urdal, H., Achilles, S., MacDowell, J., Huang, S.H., Vital, V., et al. (2019). Grid-forming inverters: Are they the key for high renewable penetration? *IEEE Power and Energy magazine*, 17(6), 89–98.

Paquette, A.D. and Divan, D.M. (2014). Virtual impedance current limiting for inverters in microgrids with synchronous generators. *IEEE Transactions on Industry Applications*, 51(2), 1630–1638.

Töpfer, M., Ahmed, N., and Weber, H. (2020). Dimensioning the internal components of a hydrogen storage power plant. In *2020 International Conference on Smart Energy Systems and Technologies (SEST)*, 1–6. IEEE.